Journal of Power Sources 184 (2008) 16–22

Contents lists available at ScienceDirect

Journal of Power Sources

journal homepage: www.elsevier.com/locate/jpowsour

Physical and electrochemical characterizations of PtPb/C catalyst prepared by pyrolysis of platinum(II) and lead(II) acetylacetonate

Zhaolin Liu*, Bing Guo, Siok Wei Tay, Liang Hong, Xinhui Zhang

Institute of Materials Research & Engineering, 3 Research Link, Singapore 117602

ARTICLE INFO

Article history:
Received 25 February 2008
Received in revised form 27 April 2008
Accepted 19 May 2008
Available online 19 June 2008

Keywords:
Platinum-lead catalyst
Platinum catalyst
Platinum-ruthenium catalyst
Formic acid oxidation
Methanol oxidation
Fuel cell

ABSTRACT

Platinum (Pt) and platinum-lead (PtPb) nanoparticles supported on Vulcan XC-72 carbon are prepared by polyalcohol reduction of platinum acetylacetonate and lead acetylacetonate in octyl ether. The catalysts are characterized by transmission electron microscopy (TEM), X-ray diffraction (XRD) and X-ray photoelectron spectroscopy (XPS). The Pt and PtPb nanoparticles, which are controlled by a capping agent added during the synthesis, have diameters of 2.5–6 nm. The Pt/C and PtPb/C catalysts display the characteristic diffraction peaks of a face-centered cubic Pt structure and the pure phase of the PtPb intermetallic, respectively. Results from XPS analysis reveal that the PtPb/C catalyst contains mostly Pt(0), Pb(0) and carbon, with traces of Pt(IV) (e.g., PtO_2) and –C═O. The electrocatalytic activity of the PtPb/C catalyst towards formic acid and methanol oxidation is investigated by cyclic voltammetry, impedance measurements and chronoamperometry. The PtPb/C catalyst has higher electrocatalytic activity for both formic acid and methanol oxidation than the Pt/C and commercially-available PtRu/C catalysts. Preliminary tests on a single cell indicate that a PtPb/C anode catalyst gives the best electrocatalytic performance among all Pt/C, PtPb/C and PtRu/C catalysts.

1. Introduction

Direct methanol fuel cells (DMFCs) are potential power sources for portable electronic devices. Challenging issues such as methanol crossover and poor methanol electro-oxidation kinetics are the main obstacles to the commercialization of DMFC technology [1–5]. Methanol crossover is the diffusion-driven phenomenon of methanol travelling through the membrane from the anode to the cathode. It affects the performance of the cathode and lowers the efficiency of a DMFC. The other issue is the slow electrochemical reaction of the DMFC. Previous research has led to the conclusion that the choice and preparation of the anode catalyst in a DMFC is far more important than in other types of fuel cell. This is because the kinetics of methanol electro-oxidation are relatively slow, namely, about six orders of magnitude lower than those of hydrogen near room temperature. Therefore, if the anode catalyst is of poor quality, a DMFC may not even operate. It has been found that the use of a second element with Pt, such as Ru, Sn, Co, Cr, Fe, and Mo, in the form of an alloy or a co-deposit yields significant improvement in the CO-tolerance relative to pure Pt. Among them, the PtRu alloy has been found to be the most active binary catalyst and is the state-of-the-art anode catalyst for DMFCs. A new approach in the search for electrocatalysts to replace PtRu with less costly materials and to avoid the inherent problems in using disordered alloys as catalysts has been reported [6]. In place of the disordered PtRu alloy, ordered intermetallic phases, such as PtBi and PtPb, exhibit high electrocatalytic activity towards formic acid and methanol oxidation and essentially complete tolerance towards poisoning by CO [7–9].

It is well known that catalytic activity is strongly dependent on the shape, size and distribution of the metal particles [10–14]. Conventional preparation techniques based on wet impregnation and chemical reduction of the metal precursors often do not provide adequate control of particle shape and size [15]. Accordingly, there are continuing efforts to develop alternative synthesis methods based on microemulsions [16], sonochemistry [17,18], or microwave irradiation [19–24]. Sun et al. [25] reported a new method for preparing monodisperse FePt nanoparticles. In this procedure, particles were synthesized by polyalcohol reduction of organometallic precursors and decomposition of metal carbonyls in high-boiling point solvents with the presence of capping agents, which are employed to control the particle size and shape. This study involves a simple synthetic approach to obtain high-activity Pt/C and PtPb/C catalysts, which are prepared by polyalcohol reduction of platinum acetylacetonate or platinum acetylacetonate and lead acetylacetonate in octyl ether in the presence of oleylamine and oleic acid.

* Corresponding author. Tel.: +65 68727532; fax: +65 68720785.
E-mail address: zl-liu@imre.a-star.edu.sg (Z. Liu).

0378-7753/$ – see front matter © 2008 Elsevier B.V. All rights reserved.
doi:10.1016/j.jpowsour.2008.05.087

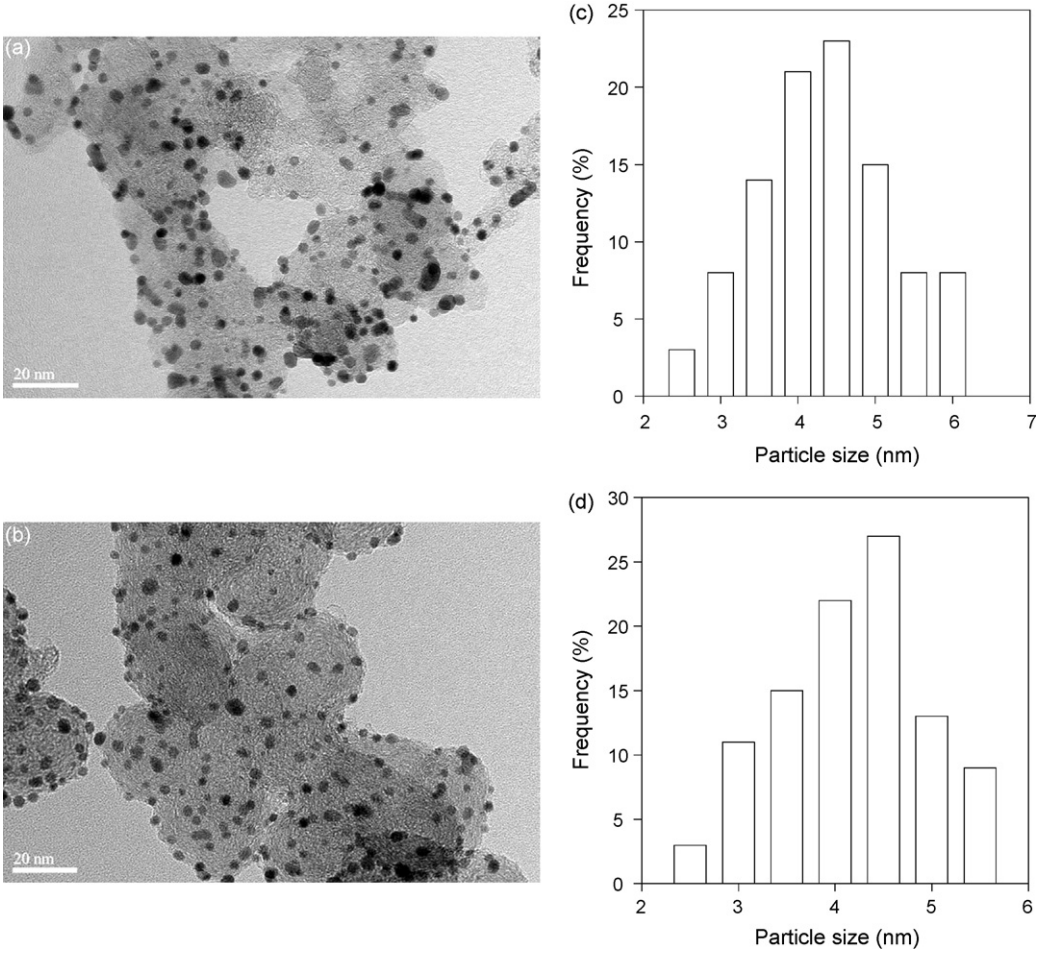

Fig. 1. TEM images of Pt/C and PtPb/C catalysts: (a) Pt/C; (b) PtPb/C; (c) particle-size distribution of Pt/C; (d) particle-size distribution of PtPb/C.

2. Experimental

2.1. Preparation of Pt/C and PtPb/C catalysts

Platinum(II) and lead(II) acetylacetonate [$Pt(acac)_2$, purity: 97%; $Pb(acac)_2$, purity: 97%], hexadecanediol (purity: 98%), oleic acid (purity: 90%), oleylamine (purity: 70%) and octyl ether (purity: 99%) were purchased from Aldrich. All reagents were used without further purification. The Pt/C and PtPb/C catalysts were synthesized by the polyol reduction of $Pt(acac)_2$ or $Pt(acac)_2$ and $Pb(acac)_2$ in a mixture of oleic acid and oleylamine under a nitrogen atmosphere. A typical preparation of the PtPb/C catalyst would consist of the following steps. 0.5 mmol of $Pb(acac)_2$, 0.5 mmol of $Pt(acac)_2$, 25 ml of octyl ether, 2.5 ml of oleic acid, 2.5 ml of oleylamine, 1.5 mmol hexadecanediol and 0.39 g of Vulcan XC-72 carbon were placed in a three-necked flask and uniformly dispersed by ultrasound at ambient temperature. The flask was then evacuated to remove oxygen and volatile components from the reaction solution. After evacuation, the flask was purged three times with argon gas. Subsequently, the temperature was raised to 240–250 °C at a heating rate of 20 °C min^{-1} under an argon atmosphere. After 30 min of reaction at 240–250 °C, the flask was cooled to 50 °C and ethanol bubbled by nitrogen was added into the flask. By centrifuging this mixture, a black powder was separated from the matrix and then redispersed in hexane. The precipitation and redispersion processes were repeated three times to remove impurities completely. Finally, the powder was dried at 60 °C under vacuum. By this synthetic procedure, 0.4 g PtPb/C catalyst capped with oleic acid were obtained.

In order to remove the stabilizing shell on the nanoparticles, the as-synthesized Pt/C and PtPb/C catalysts capped with oleic acid were heat-treated in argon for 3 h at 360 °C. The furnace was purged with argon gas for at least 15 min prior to the heat treatment. The resulting samples are identified as Pt/C and PtPb/C catalysts in the following discussion.

2.2. Characterization

To determine the actual platinum and lead contents in the PtPb/C catalyst, inductively coupled plasma spectroscopy (ICP) was used to measure the unreacted metal ions remaining in the octyl ether mixtures. The Pt:Pb atomic ratio was 1:1, which agrees exactly with the stoichiometric ratio of 1:1 used for the preparation.

The particle morphology, size, and size-distribution of the catalysts were characterized by transmission electron microscopy (TEM) using a Philips CM300 FEG system operating at 300 kV. The TEM samples were prepared by placing a drop of the sonicated (1 h) catalyst suspension in acetone on a 3 mm Cu grid, following by drying under ambient conditions. X-ray diffraction (XRD) patterns were recorded by means of Bruker GADDS diffractometer with an area detector that used a Cu Kα source (λ = 1.54056 Å) operating at 40 kV and 40 mA. The XRD samples were obtained by depositing carbon-supported nanoparticles on a glass slide and then drying overnight under vacuum. X-ray photoelectron spectroscopic (XPS)

analysis was carried out with a VG ESCALAB MKII instrument that used a Mg Kα X-ray source. The XPS samples were prepared by dispensing the sonicated catalyst suspension in acetone onto a polished graphite surface followed by drying.

2.3. Electrochemical measurements

An EG &G Model 273 potentiostat/galvanostat and a conventional three-electrode test cell were used for electrochemical measurements. The working electrode was a thin layer of Nafion-impregnated catalyst cast on a vitreous carbon disc held in a Teflon cylinder. The catalyst layer was obtained as follows: (i) a slurry was first prepared by sonicating for 1 h a mixture of 0.5 ml of deionized water, 0.06 g of Pt/C or PtPb/C catalyst, and 0.5 ml of Nafion solution (Aldrich: 5 wt.% Nafion); (ii) 7 μl of the slurry was pipetted and spread on the carbon disc; (iii) the electrode was dried at 90 °C for 1 h and mounted on a stainless-steel support. The surface area of the vitreous carbon disc was 0.25 cm^2. A Pt gauze and a Ag/AgCl electrode were used as the counter and reference electrodes, respectively. All potentials are reported with respect to the Ag/AgCl electrode. All electrolyte solutions were purged with high-purity argon for 2 h prior to each measurement. For cyclic voltammetry of formic acid or methanol oxidation, the electrolyte solution was 0.5 M HCOOH or CH_3OH in 0.5 M H_2SO_4 and was prepared from high-purity sulfuric acid, high-purity formic acid or methanol, and distilled water. The measurement of electrode impedance was performed by connecting the EG & G model 263A to an FRD-100 lock-in amplifier over a frequency range from 100 kHz to 100 mHz. Impedances were measured under potentiostatic control of the cell.

The membrane electrode assembly (MEA) for the DMFC test cell was made by hot-pressing pretreated Nafion®1135 together with an anode sheet and a cathode sheet. The anode sheet was a carbon paper (SGL, Germany) with a Pt/C or PtPb/C catalyst layer. The cathode sheet was a carbon paper with a carbon-supported 40 wt. % Pt catalyst layer supplied by E-TEK. The catalyst loadings at the anode and cathode were 8 and 4 mg cm^{-2}, respectively, and the effective electrode area was 6 cm^2. The fuel was 2 M formic acid or methanol delivered at 2 ml min^{-1} by a micropump. The oxygen flow was regulated by a flowmeter at 500 cm^3 min^{-1}.

3. Results and discussion

To prepare Pt or PtPb nanoparticles, a combination of oleic acid and oleylamine was used as a capping agent to stabilize the monodisperse Pt or PtPb nanoparticles. The synthesis is based on the reduction of $Pt(acac)_2$ and $Pb(acac)_2$ by a diol in high-temperature solutions. Fig. 1a and b is typical TEM images of the Pt/C and PtPb/C catalysts, and reveals a remarkably uniform and high dispersion of metal and alloy particles on the carbon surface. The average diameters of 4.4 nm (for Pt) and 4.2 nm (for PtPb) are accompanied by relatively narrow particle-size distributions, as shown in Fig. 1 c and d (standard deviations = 0.3 nm, from counting about 100 particles in the TEM images).

Powder X-ray diffraction patterns for the PtPb/C and Pt/C catalysts are shown in Fig. 2. The pattern of the PtPb/C catalyst indicates the formation of a pure phase of a PtPb (JCPDS database—International Centre for Diffraction Data, 1999, PCPDFWIN version 2.02); there are no peaks for Pt, Pb and other intermetallics. The XRD patterns for the Pt/C catalyst show five diffraction peaks that are indexed to the {1 1 1}, {2 0 0}, {2 2 0}, {3 1 1} and {2 2 2} planes of the Pt face-centered cubic (fcc) crystal structure. The strong diffraction at $2\theta < 30^\circ$ pertains mostly to the carbon black support.

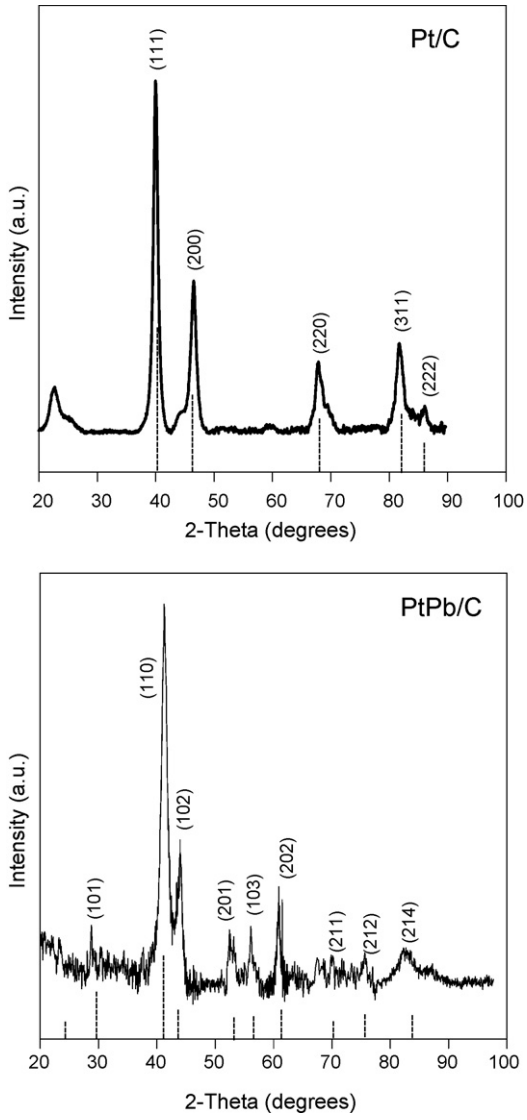

Fig. 2. Powder X-ray diffraction patterns of PtPb/C and Pt/C catalysts.

The broader diffraction peaks for the two catalysts indicate a smaller average metal or alloy particle size as calculated by the Scherrer equation [28]:

$$d(\text{Å}) = \frac{k\lambda}{\beta \cos\theta} \quad (1)$$

where k is coefficient (0.9), λ is the wavelength of the X-ray used (1.54056 Å), β is the full-width half-maximum of respective diffraction peak, and θ is the angle at the position of peak maximum. The average particle size obtained from the XRD patterns is 4.2 nm for Pt/C and 4.1 nm for PtPb/C. Thus, the values are slightly lower than those obtained above by TEM analysis.

The surface composition and chemical states of the Pt/C and PtPb/C catalysts were examined by XPS. The narrow-scan spectra in the Pt 4f, Pb 4f, O 1s, and C 1s regions for the PtPb/C catalyst are presented in Fig. 3. The Pt 4f region shows two doublets from the spin-orbital splitting of the $4f_{7/2}$ and $4f_{5/2}$ states. The main doublet at 71.1 and 74.4 eV (in a peak area ratio of 4:3) is contributed by Pt $4f_{7/2}$, and demonstrates the presence of metallic platinum Pt(0). The smaller doublet due to Pt $4f_{5/2}$ is detected at 72.1 and 75.4 eV, which indicates the presence of higher oxidation states of Pt, such as Pt(IV) (e.g., PtO_2) in the sample. This is

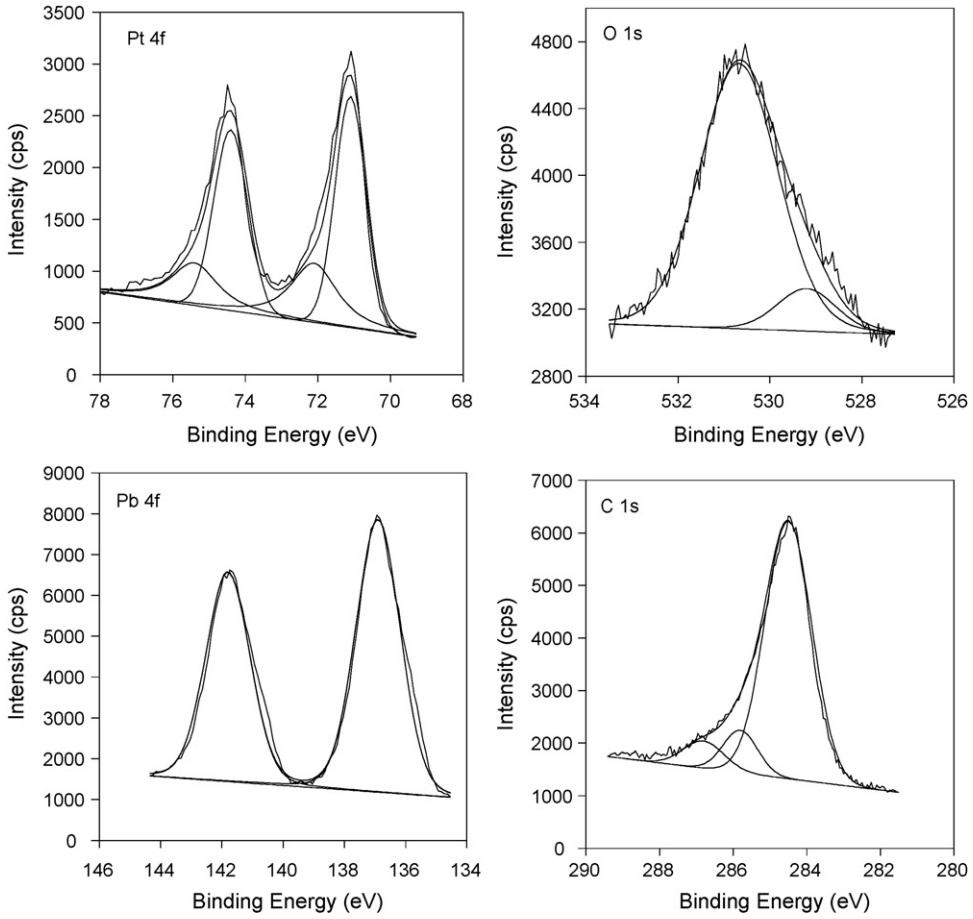

Fig. 3. XPS spectra of PtPb/C catalyst in Pt 4f, Pb 4f and C 1s region.

corroborated by the O 1s spectrum. The position of the Pb $4f_{7/2}$ and Pb $4f_{5/2}$ spectral lines for the PtPb/C catalyst occurs at 136.9 and 141.8 eV, respectively, which indicates the presence of metallic lead Pb(0) [29]. The fact that essentially the same value is found for PtPb/C suggests there is no significant modification in the binding energy arising from intermetallic compound formation. Similar behaviour has been reported for intermetallic phase PtPb and for Pb incorporated in a Pt film [30,31]. The C 1s spectrum appears to be composed of graphitic carbon (284.6 eV) and –C=O like species (285.83 eV) [29]. A small amount of surface functional groups with high oxygen contents is also noted in the spectrum (286.8 eV).

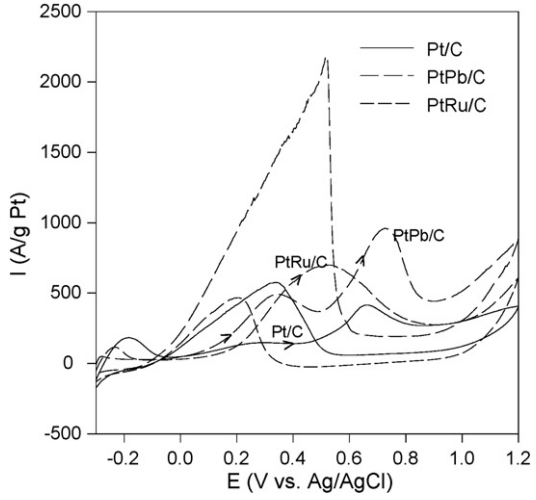

Fig. 4. Cyclic voltammograms of room temperature formic acid oxidation on three different catalyst electrodes: PtPb/C, Pt/C and PtRu alloy supported on carbon (Alfa Aesar, Pt: 20 wt.%, Ru: 10 wt.%) catalysts in 0.5 M H_2SO_4, 0.5 M formic acid at 20 mV s^{-1}.

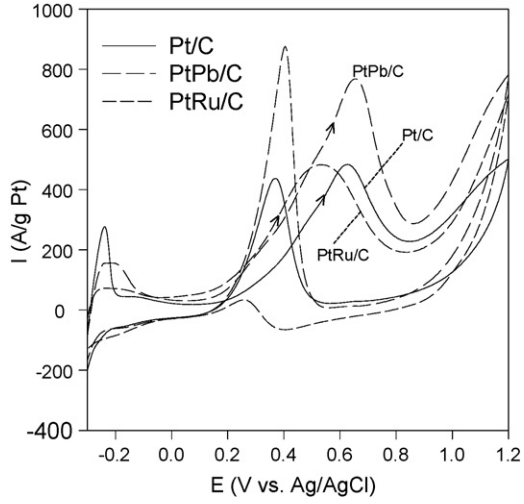

Fig. 5. Cyclic voltammograms of room temperature methanol oxidation on three different catalyst electrodes: PtPb/C, Pt/C and PtRu alloy supported on carbon (Alfa Aesar, Pt: 20 wt.%, Ru: 10 wt.%) catalysts in 0.5 M H_2SO_4, 0.5 M methanol at 20 mVs^{-1}.

Table 1
Onset potential and current densities at different forward sweeping potentials for formic acid oxidation

Catalyst	Onset potential (V)	Current density (A (g Pt)$^{-1}$)			
		0.1 V	0.2 V	0.3 V	0.4 V
Pt/C	0.00	80.7	125.9	146.9	139.5
PtPb/C	−0.10	104.8	238.1	453.7	448.3
PtRu/C(Alfa Aesar)	0.05	52.5	121.6	342.2	578.2

Cyclic voltammograms of formic acid oxidation on different catalyst electrodes are presented in Fig. 4. A commercial PtRu alloy catalyst (supported on Vulcan XC-72, Pt: 20 wt.%, Ru: 10 wt.%, Alfa Aesar) was also tested for comparison. For the Pt/C and PtPb/C catalysts, two anodic peaks in the forward scan are one peak in the reverse scan are observed, which shows the similarity in the voltammetric characteristics of the two catalysis. The reaction commences in the hydrogen region and proceeds slowly during the forward scan to reach a plateau or peak at around 0.3 V. This corresponds to formic acid oxidation via a dehydrogenation path, but the coverage by CO_{ads} simultaneously continues to grow and causes only relatively small currents [26]. At potentials more positive than 0.6 V, the reaction becomes significantly accelerated and an anodic peak emerges at 0.7 V. The latter can be attributed to the oxidative removal of CO_{ads} together with oxidation of formic acid on sites that were previously blocked by CO_{ads}. At higher potentials, formic acid oxidation is deactivated as result of Pt surface oxidation. On reversing the potential scan, the surface remains inactive until partial reduction of the irreversibly formed surface oxides. One cathodic peak near 0.4 V is observed, and is due to formic acid oxidation after reduction of Pt oxides. For the PtRu/C catalyst, there is only one anodic peak in the forward scan, which indicates its different voltammetric characteristic and mechanism of formic acid oxidation compared with the Pt/C and PtPb/C catalysts. The onset potentials and current densities at different forward

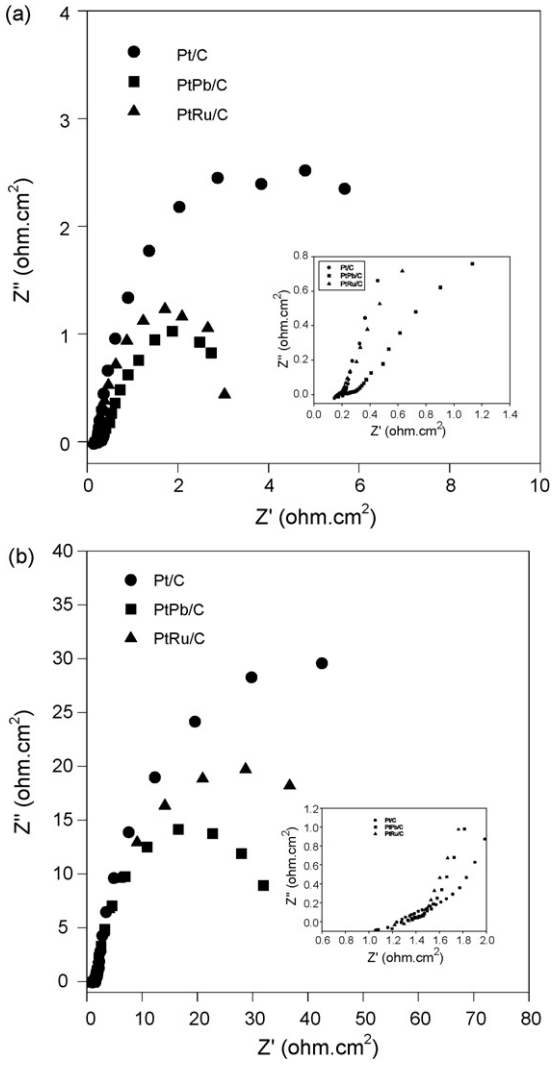

Fig. 6. Electrochemical impedance spectroscopy of PtPb/C, Pt/C and PtRu alloy supported on carbon (Alfa Aesar, Pt: 20 wt.%, Ru: 10 wt.%) catalysts at electrode potential of 0.2 V in (a) 0.5 M H_2SO_4, 0.5 M formic acid and (b) 0.5 M H_2SO_4, 0.5 M methanol. Amplitude of modulation potential is 10 mV. Frequency is changed from 100 kHz to 100 mHz.

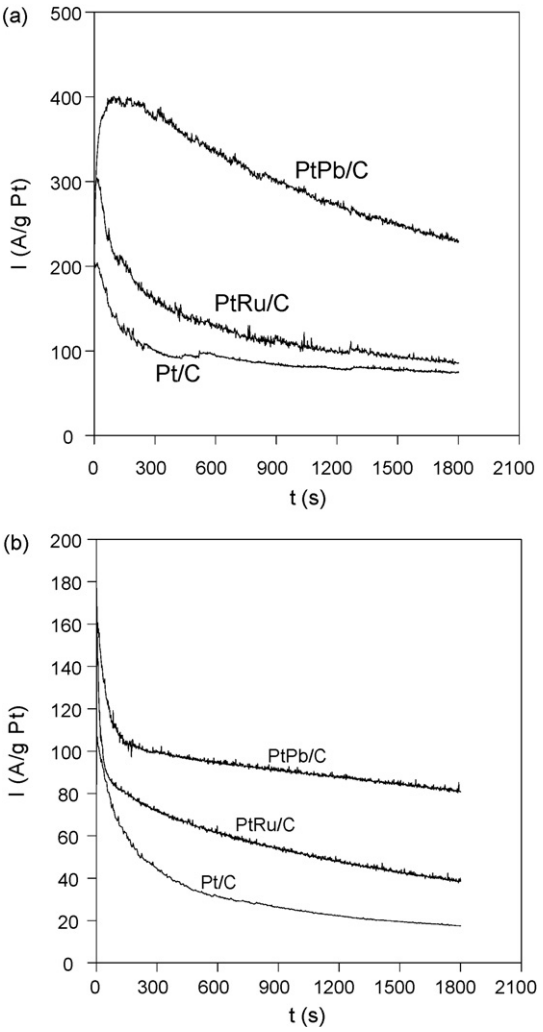

Fig. 7. Chronoamperometric measurements of PtPb/C, Pt/C and PtRu alloy supported on carbon (Alfa Aesar, Pt: 20 wt.%, Ru: 10 wt.%) catalysts (a) at electrode potential of 0.3 V in 0.5 M H_2SO_4, 0.5 M formic acid and (b) at electrode potential of 0.4 V in 0.5 M H_2SO_4, 0.5 M methanol.

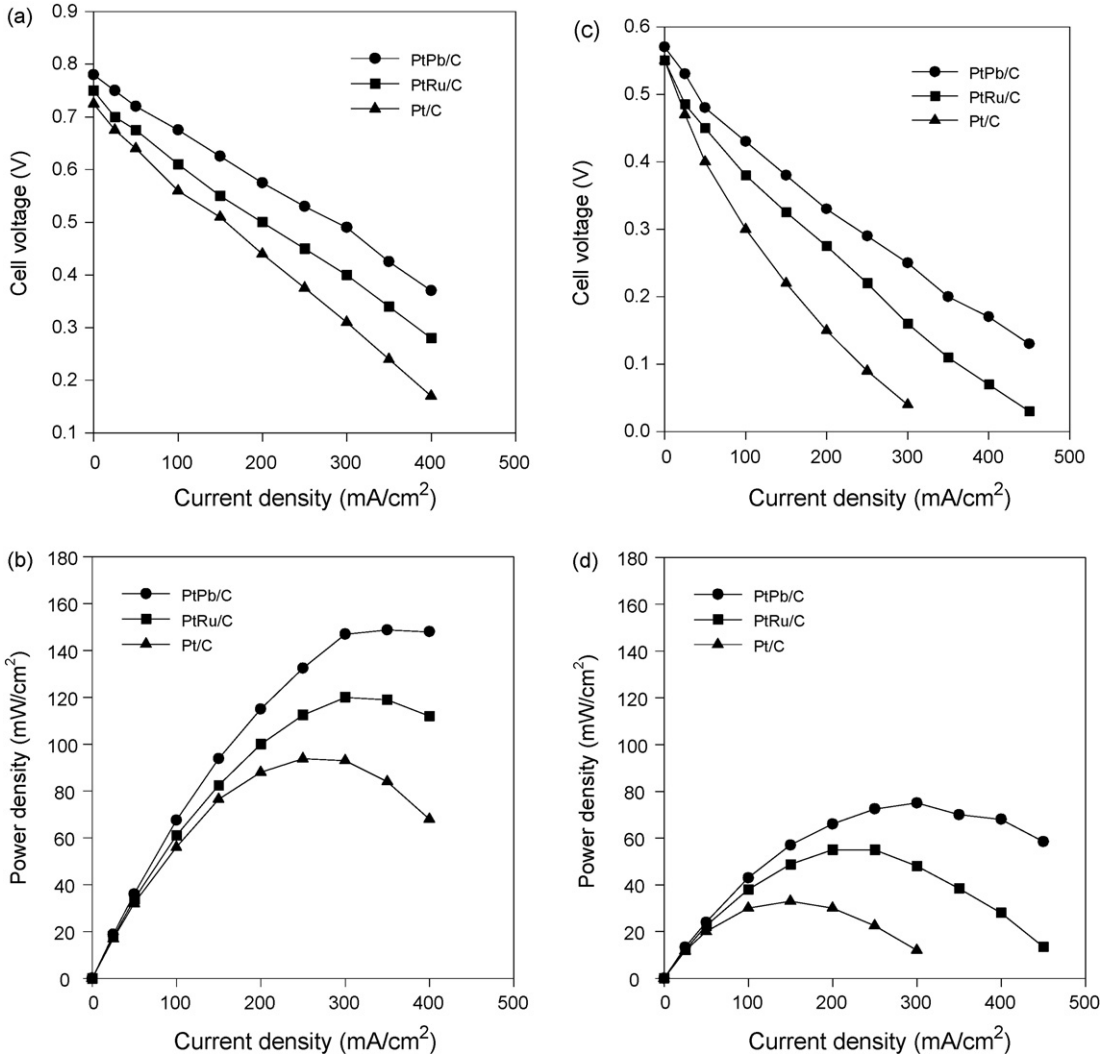

Fig. 8. Polarization curves and output powers of single cell at operating temperature of 70 °C. Cathode: Pt/C (E-TEK) (4 mg cm^{-2}), O_2 500 cm^3 min^{-1}; Anode: catalyst loading, 8 mg cm^{-2}. (a and b) 2 M formic acid, 2 ml min^{-1}; (c and d) 2 M methanol, 2 ml min^{-1}.

sweeping potentials for formic acid oxidation are summarized in Table 1. The onset potential on a PtPb/C catalyst is detected at −0.1 V, whereas it occurs at 0 and 0.05 V for Pt/C and PtRu/C catalysts, respectively. A good catalyst for formic acid oxidation is one that exhibits a low onset potential. This implies that the PtPb/C catalyst may have superior electrocatalytic activity compared with the Pt/C and PtRu/C catalysts. It is seen from Fig. 4 and Table 1 that the PtPb/C catalyst gives a higher current density of formic acid oxidation than the Pt/C catalyst both in the forward and reverse scan. Similarly, the PtPb/C catalyst exhibits higher current density compared with the PtRu/C catalyst in the forward scan before 0.35 V. The PtRu/C catalyst gives a higher current density of formic acid oxidation between 0.35 and 0.6 V. Afterwards, a higher peak at 0.75 V for the PtPb/C catalyst is observed. This suggests that the presence of lead in the PtPb nanoparticles catalyst markedly enhances the electrocatalytic activity of platinum towards formic acid oxidation.

Cyclic voltammograms of methanol oxidation on different catalyst electrodes are shown in Fig. 5. There is no significant difference in any feature between the volammograms of methanol oxidation on PtPb/C and Pt/C catalysts. In the forward scan, methanol oxidation produces a prominent symmetric anodic peak at around 0.6 V for the Pt/C and PtPb/C catalysts and at 0.5 V for the PtRu/C catalyst. The peak current density of methanol oxidation for the PtPb/C catalyst is higher than that for Pt/C and PtRu/C catalysts. In the reverse scan, an anodic peak current density is detected at around 0.4 V for the Pt/C and PtPb/C catalysts and at 0.3 V for the PtRu/C catalyst. Manohara and Goodenough [27] attributed this anodic peak in the reverse scan to the removal of the incompletely oxidized carbonaceous species formed in the forward scan. These carbonaceous species are mostly in the form of linearly bonded Pt=C=O. Table 2 summarizes the onset potentials and current densities at different forward sweeping potentials for methanol oxidation. From the values presented in Table 2, the Pt/C, PtPb/C and PtRu/C catalysts showed onset potentials of 0.18, 0.10 and 0.10 V, respectively. The PtPb/C and PtRu/C catalysts have the same onset potential for methanol oxidation. It is observed from Fig. 5 and Table 2 that the

Table 2
Onset potential and current densities at different forward sweeping potentials for methanol oxidation

Catalyst	Onset potential (V)	Current density (A (g Pt)$^{-1}$)			
		0.3 V	0.4 V	0.5 V	0.6 V
Pt/C	0.18	90.1	179.6	319.1	466.0
PtPb/C	0.10	182.3	304.1	485.7	676.2
PtRu/C (Alfa Aesar)	0.10	191.2	348.3	474.8	449.0

PtPb/C catalyst exhibits a higher current density of the methanol oxidation compared with the Pt/C and PtRu/C catalysts, both in the forward scan and reverse scan.

Nyquist plots of PtPb/C and Pt/C catalysts for formic acid and methanol oxidation are shown in Fig. 6. The inserts of Fig. 6 are the Nyquist plots in the range of high frequency. The frequency is changed from 100 kHz to 100 mHz. As shown in Fig. 6, the impedances on both the imaginary and real axes of the PtPb/C catalyst are lower than those of the Pt/C and PtRu/C catalysts. This indicates low electrochemical polarization impedances of the PtPb/C catalyst compared with those of Pt/C and PtRu/C catalysts. For all samples, very small arcs in the range of high frequency indicate very weak ohm polarization impedances. In addition, in the range of low frequency, electrochemical polarization impedances of PtPb/C catalyst are lower than those of Pt/C and PtRu/C catalysts. These results confirm that the PtPb/C catalyst presents a lower charge-transfer resistance compared with the Pt/C and PtRu/C catalysts and its activity towards formic acid and methanol oxidation is enhanced by addition of lead in Pt.

The PtPb/C, Pt/C and PtRu/C catalysts were biased at 0.3 V for formic acid oxidation and at 0.4 V for methanol oxidation and the changes in their polarization currents with time were recorded (Fig. 7). The PtPb/C catalyst for both formic acid and methanol oxidation is able to maintain the highest current density among all the catalysts at all corresponding potentials, indicating enhanced electrocatalytic activities compared with Pt/C and PtRu/C catalysts. At 0.3 V, the current density of PtPb/C catalyst for formic acid oxidation is about three times higher than that for the PtRu/C catalyst. Formic acid oxidation obeys a dual-path mechanism [32–34], namely: (i) dehydrogenation in which formic acid is oxidized directly into CO_2; (ii) dehydration, which involves the CO_{ads} intermediate. The oxidative removal of CO_{ads} occurs at higher potentials. The higher electroactivity of the PtPb/C catalyst towards formic acid oxidation suggests that it promotes dehydrogenation without the formation of a surface-poisoning CO_{ads} intermediate. At 0.4 V, the PtPb/C catalyst for methanol oxidation gives a current density which is about twice that for the PtRu/C catalyst.

Polarization and power density curves of single cells with PtPb/C, Pt/C and PtRu/C catalysts as anode catalysts are shown in Fig. 8. As identified in the cyclic voltammetry and chronoamperometry tests, the PtPb/C catalyst gives the highest activity among the three catalysts. The peak power densities using Pt/C, PtRu/C and PtPb/C catalysts for formic acid oxidation are 90, 120 and 148 mW cm^{-2}, respectively, whereas the corresponding peak power densities are 32, 55 and 75 mW cm^{-2} for methanol oxidation.

4. Conclusions

Pt and PtPb nanoparticles supported on Vulcan XC-72 carbon have been prepared by polyalcohol reduction of platinum acetylacetonate or platinum acetylacetonate and lead acetylacetonate in octyl ether with the presence of oleylamine and oleic acid. The Pt and PtPb particles are nanosized and have relatively narrow particle-size distributions. X-ray diffraction patterns show that the Pt/C and PtPb/C catalysts display the characteristic diffraction peaks of a face-centered cubic Pt structure and the pure phase of PtPb intermetallic, respectively. Results from XPS analysis reveal that the PtPb/C catalyst contains mostly Pt(0), Pb(0) and carbon, with traces of Pt(IV) (e.g., PtO_2) and –C=O. The PtPb/C catalyst displays enhanced electrocatalytic activity towards both formic acid and methanol oxidation compared with Pt/C and commercially-available PtRu/C catalysts. Preliminary data from a single cell using the PtPb/C as an anode catalyst delivers high power density.

References

[1] S. Wasmus, A. Kuver, J. Electroanal. Chem. 461 (1999) 14.
[2] X. Ren, P. Zelenay, S. Thomas, J. Davey, S. Gottesfeld, J. Power Sources 86 (2000) 11.
[3] J.G. Liu, T.S. Zhao, R. Chen, C.W. Wong, Electrochem. Commun. 7 (2005) 288.
[4] Z.L. Liu, J.Y. Lee, M. Han, W.X. Chen, L.M. Gan, Langmuir 20 (2004) 181.
[5] J. Prabhuran, T.S. Zhao, H. Yang, J. Electroanal. Chem. 578 (2005) 105.
[6] D. Volpe, E. Casado-Rivera, L. Alden, C. Alden, C. Lind, K. Hagerdon, C. Downie, C. Korzeniewski, F.J. DiSalvo, H.D. Abruña, J. Electrochem. Soc. 151 (2004) A971.
[7] C. Roychowdhury, F. Matsumoto, V.B. Zeldovich, S.C. Warren, P.F. Mutolo, M. Ballesteros, U. Wiesner, H.D. Abruña, F.J. DiSalvo, Chem. Mater. 18 (2006) 3365.
[8] L.R. Alden, C. Roychowdhury, F. Matsumoto, D.K. Han, V.B. Zeldovich, H.D. Abruña, F.J. DiSalvo, Langmuir 22 (2006) 10465.
[9] S. Maksimuk, S. Yang, Z. Peng, H. Yang, J. Am. Chem. Soc. 129 (2007) 8684.
[10] S. Link, A. Beeby, S. FitzGerald, M.A. El-Sayed, T.G. Schaaff, R.L. Whetten, J. Phys. Chem. B 106 (2002) 3410.
[11] G.H. Woehrle, M.G. Warner, J.E. Hutchison, J. Phys. Chem. B 106 (2002) 9979.
[12] Y. Yang, S. Chen, Nano Lett. 3 (2003) 75.
[13] Y. Negishi, T. Tsukuda, J. Am. Chem. Soc. 125 (2003) 4063.
[14] J.P. Wilcoxon, P. Provencio, J. Phys. Chem. B 107 (2003) 12949.
[15] I.S. Armadi, Z.L. Wang, T.C. Green, A. Henglein, M.A. Ei-Sayed, Science 272 (1996) 1924.
[16] Z.L. Liu, J.Y. Lee, M. Han, W.X. Chen, L.M. Gan, J. Mater. Chem. 12 (2002) 2453.
[17] K. Okitsu, A. Yue, S. Tanabe, H. Matsumoto, Chem. Mater. 12 (2000) 3006.
[18] T. Fujimoto, S. Teraushi, H. Umehara, I. Kojima, W. Henderson, Chem. Mater. 13 (2001) 1057.
[19] W.Y. Yu, W.X. Tu, H.F. Liu, Langmuir 15 (1999) 6.
[20] W.X. Tu, H.F. Liu, Chem. Mater. 12 (2000) 564.
[21] S. Komarneni, D.S. Li, B. Newalkar, H. Katsuki, A.S. Bhalla, Langmuir 18 (2002) 5959.
[22] W.X. Chen, J.Y. Lee, Z.L. Liu, Chem. Commun. (2002) 2588.
[23] Z.L. Liu, J.Y. Lee, W.X. Chen, M. Han, L.M. Gan, Langmuir 20 (2004) 181.
[24] J. Huang, Z. Liu, X. Liu, C. He, S.Y. Chow, J. Pan, Langmuir 21 (2005) 699.
[25] S. Sun, C.B. Murray, D. Weller, L. Folks, A. Moser, Science 287 (2000) 1989.
[26] V.M. Jovanovic, D. Tripkovic, A. Tripkovic, A. Kowal, J. Stoch, Electrochem. Commun. 7 (2005) 1039.
[27] R. Manohara, J.B. Goodenough, J. Mater. Chem. 2 (1992) 875.
[28] B.E. Warren, X-ray Diffraction, Addison-Wesley, Reading, MA, USA, 1996.
[29] J.F. Moulder, W.F. Stickle, P.E. Sobol, K.D. Bomben, Handbook of X-ray Photoelectron Spectroscopy, Perkin-Elmer, USA, 1992.
[30] D.R. Blasini, D. Rochefort, E. Fachini, L.R. Alden, F.J. DiSalvo, C.R. Cabrera, H.D. Abruña, Surf. Sci. 600 (2006) 2670.
[31] A. Palermo, F.J. Williams, R.M. Lambert, J. Phys. Chem. B 106 (2002) 10215.
[32] A. Capon, R. Parsons, J. Electroanal. Chem. 45 (1973) 205.
[33] G.Q. Lu, A. Crown, A. Wieckowski, J. Phys. Chem. B 103 (1999) 9700.
[34] R.S. Jayashree, J.S. Spendelow, J. Yeom, C. Rastogi, M.A. Shannon, P.J.A. Kenis, Electrochimica Acta 50 (2005) 4674.